Int. J. Heat Mass Transfer. Vol. 30, No. 10, pp. 2059–2071, 1987
Printed in Great Britain

0017–9310/87 $3.00 + 0.00

Statistical and spectral properties of tracer concentration in round buoyant jets

PANOS N. PAPANICOLAOU and E. JOHN LIST
W. M. Keck Laboratory of Hydraulics and Water Resources, California Institute of Technology, Pasadena, CA 91125, U.S.A.

(*Received* 5 *June* 1986 *and in final form* 27 *February* 1987)

Abstract—Spatial growth, temperature decay, and turbulence structure have been studied experimentally in axially-symmetric buoyant jets in transition to plumes and in fully developed plume flows. Temperature records obtained with fast response thermistors located in these flows form the basis for the study. The results obtained support previous asymptotic arguments pertaining to the rate of decay of mean temperature and r.m.s. temperature fluctuations. Spectral energy distributions in jets and plumes show that the evolution from buoyant jets to plumes is characterized by a significant shift in the wave number distribution of temperature variance density.

1. INTRODUCTION

TURBULENT jets in which the discharged fluid differs in density from the ambient fluid are termed buoyant jets. They occur somewhat rarely in nature but are observed in active volcanoes and the recently discussed 'black smokers' discovered in association with rift zones in the seafloor. Plumes, on the other hand, are created by a source of buoyancy that has no inherent momentum flux, for example fires and heated surfaces. It is easily shown that at some distance from the plume source, where the initial geometry no longer has any measurable influence on the flow, buoyant jets and plumes are essentially indistinguishable. In other words, buoyant jets and plumes share a common asymptotic state. The development of buoyant jets into plumes is of significant technical interest in that engineered buoyant jets are frequently used as a disposal and dispersal mechanism for society's residuals, for example, smoke stacks and ocean outfalls.

In this paper the results of a laboratory study of the development of round buoyant jets into plumes is presented. The buoyant jets created have differing levels of initial momentum flux and buoyancy flux so that the characterization of the motion in dimensionless terms leads to an analysis of the results that clearly demonstrates this asymptotic development.

Buoyant jets (Fig. 1) can be parameterized in terms of their specific (i.e. per unit mass) fluxes of mass, momentum and density deficiency (or buoyancy flux). If Q is the volume rate of flow or specific mass flux, M the specific momentum flux, and B the specific buoyancy flux the following definitions relate Q, M and B to the usual jet parameters of diameter, mean velocity and density deficiency:

$$Q = (\pi D^2/4)W \quad [L^3T^{-1}]$$
$$M = QW \quad [L^4T^{-2}] \qquad (1)$$
$$B = Q\frac{(\rho_a - \rho_j)g}{\rho_a} \quad [L^4T^{-3}].$$

From these quantities two characteristic length scales are defined

$$l_Q = \frac{Q}{M^{1/2}} \quad \text{and} \quad l_M = \frac{M^{3/4}}{B^{1/2}}. \qquad (2)$$

The first, l_Q, defines the initial jet size, l_M is the plume equivalent of the Monin–Obukhov length scale and defines how far from a buoyant jet origin the buoyancy forces become significant. When there is no initial buoyancy flux, i.e. B is zero or vanishingly small, the motion is controlled solely by the jet momentum flux and there is no asymptotic length scale and the motion is defined as a jet. The ratio of these two length scales defines the jet Richardson number

$$R_0 = \frac{l_Q}{l_M} = \frac{QB^{1/2}}{M^{5/4}} = \left(\frac{\pi}{4}\right)^{1/4} F^{-1} \qquad (3)$$

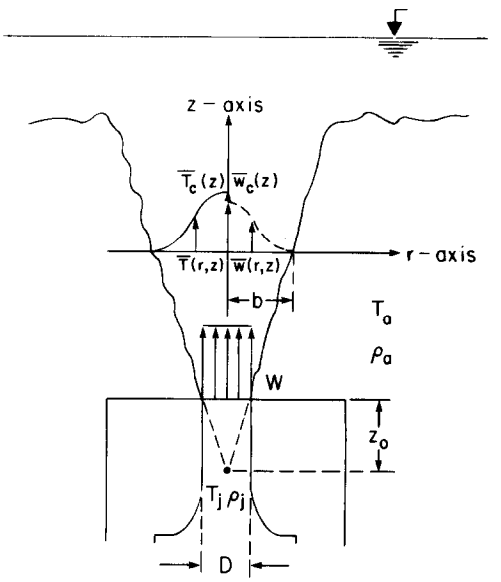

FIG. 1. Geometry of a buoyant jet—definition sketch.

NOMENCLATURE

B	specific buoyancy flux
b_T	jet lateral dimension where $\bar{T} = 0.37\bar{T}_c$
b_w	jet lateral dimension where $\bar{w} = 0.37\bar{w}_c$
D	jet diameter (dimension) at orifice
F	jet densimetric Froude number, $W/\sqrt{(g'_0 D)}$
f_R	frequency of hot–cold interface crossing
g	gravitational acceleration
g'_0	$[(\rho_j - \rho_a)/\rho_a]g$
l_M	characteristic length scale, $M^{3/4}/B^{1/2}$
l_Q	characteristic length scale, $Q/M^{1/2}$
M	jet specific momentum flux
$P(x)$	probability
Q	jet volume flux at the orifice
R_0	initial jet Richardson number
r	radial distance from the jet axis
$T(r,z)$	temperature at point (r,z)
T_j	temperature at jet exit
$\bar{T}_c$	mean excess temperature at jet centerline
T_a	ambient uniform temperature
T_0	$T_j - T_a$
t	time
W	jet exit velocity
$\bar{w}(r,z)$	time averaged axial velocity at (r,z)
z	axial distance from jet origin
z_0	location of the jet virtual origin.

Greek symbols

γ	intermittency factor
δ	differential
ρ	density
ρ_j	initial jet density
ρ_a	ambient fluid density.

Superscripts and subscripts

$(\bar{})$	time average
$(')$	deviation from a time averaged mean
$()_c$	centerline value
$()_{0,j}$	initial jet characteristic value
$()_a$	ambient fluid characteristic value.

where F is often referred to as the densimetric Froude number. The Richardson number defines the initial degree of plume behavior of a buoyant jet. If R_0 is zero the flow is a jet whereas if R_0 is of order unity (actually 0.6, see later) then the flow is plumelike. From the fact that B may be quite small in liquid flows with a modest temperature increment it is possible to use temperature as a tracer in both jets and plumes. For example, if T_0 is the temperature difference between the discharge and ambient fluids and $\bar{T}_c$ is the time-averaged mean excess temperature on the jet or plume axis, then dimensional arguments lead to the following asymptotic relations for the jet temperature:

$$\frac{(T_0/\bar{T}_c)Q}{z\sqrt{M}} = \text{constant}, \quad z \ll l_M$$

and plume temperature

$$\frac{(T_0/\bar{T}_c)Q}{z\sqrt{M}} \sim \left(\frac{z}{l_M}\right)^{2/3}, \quad z \gg l_M.$$

More detailed dimensional arguments are discussed in the works of Morton *et al.* [1], Batchelor [2] and Fischer *et al.* [3].

There are a large number of experimental investigations of turbulent jets, while the published work on plumes is very limited. Furthermore, in the case of a heated jet driven by both initial momentum and buoyancy, most authors have not defined the degree of the plume-like behavior of the flow they have measured. For jets the distribution of a scalar, such as temperature or dye concentration, has been measured by various investigators.

Probe based techniques have been applied to the measurement of tracer mixing in a jet flow field since the early 1940s. Such representative works are published by Corrsin [4], Corrsin and Uberoi [5], Hinze and van der Hegge Zijnen [6], Forstall and Gaylord [7], Sunavala *et al.* [8], Kiser [9], Wilson and Danckwerts [10], Chevray and Tutu [11] and Sforza and Mons [12]. Their results for the distribution of both mean and turbulent quantities vary within a wide range. Antonia *et al.* [13] measured velocities and temperatures conditionally in a heated jet with a coflowing stream using $\times$-wire anemometers 59 diameters from the origin. Becker *et al.* [14, 15] and Birch *et al.* [16] measured concentrations in an air jet using light scattering techniques and Raman spectroscopy, respectively. They both performed measurements up to 80 jet diameters. Shaughnessy and Morton [17] also measured concentrations in a jet at up to 50 diameters from the source in a coflowing stream using a light scattering technique. The above techniques were found to be more powerful than probe based techniques because measurements could be made at the low concentrations occurring beyond 40 jet diameters downstream from the jet origin.

Available experimental data in the plume regime are very limited and somewhat contradictory. Rouse *et al.* [18] measured temperatures and velocities above a fire generated plume. Compared to results of other

investigators their measurements appear to be more representative of the transition from jets to plumes rather than the plume regime. The local plume Richardson number calculated from their results for plane plumes was found to be 0.56, lower than 0.63 measured by Kotsovinos and List [19] and Papanicolaou [20] in plane and round plumes, respectively. Nakagome and Hirata [21] and George *et al.* [22] measured velocities and temperatures in a heated 'plume' at up to 15 plume diameters from the source. Both investigations showed that the half width of the mean velocity profile exceeded the mean concentration profile, contrary to what Rouse *et al.* [18] and other investigators found. Those authors also assumed the plume to be self similar, although it can be shown that the flows they studied were barely into the plume regime. Wygnanski and Fiedler [23] and Birch *et al.* [16] for example, showed that self similarity in velocity and concentration in jets is obtained at about 40 jet diameters from the source. Abraham [24] measured salt concentration in a 'plume' using a conductivity probe technique. His results are also representative of the transition from jets to plumes rather than the plume regime. Zimin and Frik [25] used a refractive index change based technique to measure temperatures in a plume at 13–38 diameters from the source. A virtual plume origin was determined at 12.50 jet diameters upstream from the jet nozzle, which is somewhat unusual in relation to the results of the other investigators. Ogino *et al.* [26] measured the decay of velocity and temperature along the axis of a heated buoyant jet. If their parameters are scaled according to Chen and Rodi [27] their results incorporate all three regimes; jets, transition and plumes up to about 18 characteristic length scales l_M downstream from the jet nozzle. Kotsovinos [28] has performed the most recent temperature measurements in a round buoyant jet. His axial measurements extended to about 24 l_M, but he did not perform cross-sectional measurements beyond 10 l_M. Using data from other investigators as well as his own measurements he shows that the jet growth $b_T(z)/z$ is constant up to about 12 l_M.

In summary, the available data from previous experimental studies do confirm the basic features of the dimensional analysis. However, there is significant deviation in the values of the 'universal' constants determined by different experiments. In the plume regime results such as the width ratio b_T/b_w and the local plume Richardson numbers are still equivocal. It is believed that this results from the fact that most experimental data have been obtained in the near source region where self-similar plume behavior is not well defined.

The scope of the present experimental work is the measurement of the temperature distribution in a round buoyant jet that extends well into both the jet and plume regimes. The buoyant jet behavior at a point of the flow field is defined in terms of the relative distance z/l_M which establishes clearly the flow regime under consideration.

2. THE EXPERIMENTAL SET-UP

Experiments were conducted in a vertical tank as shown in Fig. 2. The top part was rectangular in section measuring 125 × 110 cm and 95 cm deep. Four 1.125 cm thick plexiglass windows covered all four sides and provided adequate visibility to allow a thermistor probe rake to be properly aligned with the jet centerline. The bottom section of the tank was constructed from 0.634 cm thick galvanized steel plate, with a square cross-section 120 cm deep and varying in area from 110 × 110 cm (top) to 73 × 73 cm (bottom).

The jet source was supported inside the tank by four slotted steel angles which allowed a range of vertical movement. The 38.1 cm long jet consisted of two concentric cylinders with 12.7 and 7.6 cm inside diameters. The air-gap between the cylinders provided insulation of the heated jet chamber from the ambient water and thus prevented generation of a secondary plume. A calibrated thermistor probe located inside the jet source provided continuous information about the jet fluid temperature throughout the experiment. Its calibration was checked weekly and it did not drift during the period that the experiments were carried out. The base of the jet cylinder was fabricated to fit the hot water supply 1.9 cm PVC hose. The upper section was constructed to fit jet nozzles of different sizes. The jet nozzle provided a smooth transition from the inner cylinder to the jet exit and therefore generated a uniform velocity distribution at the jet exit. A flow-meter installed in line with the jet hot water supply provided continuous information on the hot water discharge rate.

The jet water supply, consisting of a heater, a hot water supply tank and a constant head tank and hoses, was properly insulated to avoid possible heat losses. Thus the initial jet condition M and B did not vary over the course of the experiment.

Temperatures were measured simultaneously at six or eight points at the same elevation z from the jet nozzle using a rake of six or eight fast response thermistor probes. The distance between two neighboring thermistor probes varied from 2 to 4 cm. The probe tips were fast response (0.014 s) glass bead thermistors (manufactured by Thermometrics) with a 0.2 mm sensitive tip with a probe resistance varying from 2.5 to 3.0 kΩ. The temperature signal from the thermistor probes (differential voltage output) was amplified, converted into digital form and stored on a diskette for subsequent data reduction by a PDP 11/60 minicomputer. The optimum sampling frequency was found to be 20 samples per second (20 Hz) per channel (probe), and the sampling period was longer than 100 s, as Kotsovinos [29], Lueck *et al.* [30] and Gregg and Meagher [31] have suggested. The energy spectrum (discussed later) also indicated that in highly turbulent regions of the buoyant jet the optimum sampling frequency should be around 20 Hz. Each thermistor probe was calibrated separately for an expected tem-

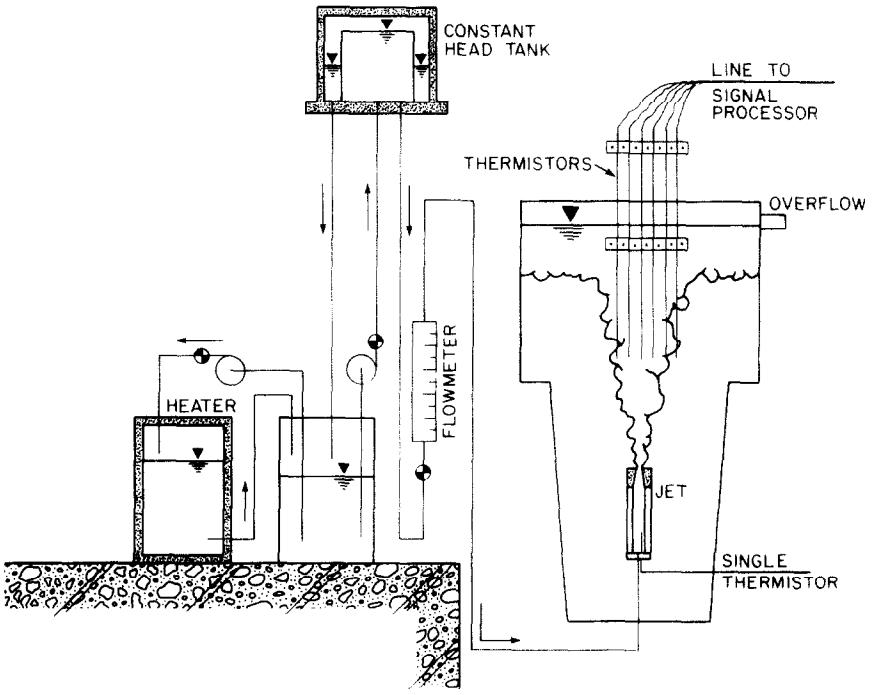

FIG. 2. Experimental set-up, plexiglass wall tank vertical section.

perature range (T_a, T_a+20)°C using a fifth-order polynomial. The combined error in the measurement of the temperature due to calibration and signal digitization was at most 0.05°C. The jet exit Reynolds number varied from 1670 for plumes to about 16 700 for jets.

The jet specific momentum and buoyancy fluxes were fixed for each experiment. The jet flow rate and temperature could be adjusted so that for a given jet diameter D and measurement elevation z the parameter z/l_M took a value in the desired range of measurement. Hence, experiments could be carried out for a wide range of z/l_M so that jet, plume and transition flows were investigated. The ambient water temperature was measured using a standard thermometer. The continuous voltage output from the thermistor probe inside the jet was read by a digital voltmeter with an accuracy of 0.01 V, which corresponded to 0.05°C, and the jet temperature was determined from a calibration curve. Data sampling was started after the jet temperature reached a steady state (in about 2 min). Temperatures were then measured in the plume with the thermistor rake located in two or three different radial positions at the same elevation. A typical simultaneous time signal from five thermistor probes is shown in Fig. 3. Thus a large number of data points were obtained at different radial distances from the jet centerline. The ambient water temperature was also measured at the beginning and the end of each experiment using all thermistor probes to ensure that the hot water interface did not reach the elevation of measurement. All thermistor probes were located in the same vertical plane through the jet centerline with their tips at the same axial distance from the nozzle.

3. EXPERIMENTAL RESULTS

A total of 32 experiments were performed and Table 1 contains the initial and measured jet parameters

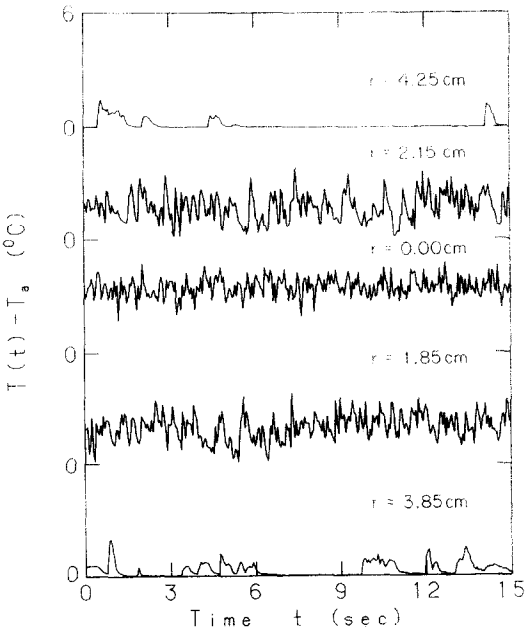

FIG. 3. Time records of the temperature measured simultaneously at five points in a jet at $z/D = 26.67$.

for all experiments. The data listed are: z (cm) the elevation from the jet nozzle at which measurements were performed, D (cm) the jet diameter, W (cm s^{-1}) jet exit velocity, T_a (°C) the ambient water temperature, T_j (°C) the jet water temperature $g'_0 = (\rho_a - \rho_j)g/\rho_a$ (cm s^{-2}) the reduced gravity at the jet exit, l_M (cm) the jet momentum length scale, and Re the jet Reynolds number. The measured quantities at elevation z from the jet nozzle are $\bar{T}_c$ the time averaged excess (above ambient) temperature (°C) on the jet axis, $\sqrt{(\overline{T_c'^2})}$ the r.m.s. temperature (°C) at the jet centerline, and b_T (cm) the 1/e temperature width of the jet. The jet width was calculated from a least square Gaussian curve fitted to the transverse time-averaged excess temperature profiles.

3.1. *Centerline temperature decay and jet growth*

The dimensionless mean excess (above the ambient) temperature $(T_0/\bar{T}_c)Q/(z\sqrt{M})$ is plotted in Fig. 4 as a function of the dimensionless elevation from the jet nozzle z/l_M. It is obvious that the mean centerline temperature decay is in accordance with the dimensional results presented earlier. The constants of proportionality and the two characteristic flow regimes are summarized as follows:

$$\frac{z}{l_M} < 1; \quad \frac{(T_0/\bar{T}_c)Q}{z\sqrt{M}} = 0.165 \qquad \text{(jet)}$$

$$\frac{z}{l_M} > 5; \quad \frac{(T_0/\bar{T}_c)Q}{z\sqrt{M}} = 0.090\left(\frac{z}{l_M}\right)^{2/3} \qquad \text{(plume).} \tag{4}$$

Fischer *et al.* [3] suggest the numerical values of the constants as 0.175 for a jet and 0.110 for a plume from the data reported by George *et al.* [22]. However, the plume constant here agrees with the 0.091 proposed by Rouse *et al.* [18]. In the interval $1 < z/l_M < 5$ jets are in transition to plumes and the buoyancy produced momentum becomes significant. At about $z/l_M > 5$, the momentum flux generated by the buoyancy exceeds by a significant margin the initial momentum flux and the asymptotic plume regime is attained.

The normalized r.m.s. values of the temperature along the jet axis also follow the trend of the time-averaged mean values, i.e.

$$\frac{(T_0/\sqrt{(\overline{T'^2})})Q}{z\sqrt{M}} = \text{constant}, \quad \text{for} \quad z/l_M < 5 \tag{5}$$

Table 1. Initial jet parameters and measured characteristic quantities for each experiment

	D	z	T_j	T_a	W	l_M	Re	g'_0	$\bar{T}_c$	$\sqrt{(\overline{T_c'^2})}$	b_T
TEM1	1.25	40	52.5	24.40	32.19	10.64	7890	10.191	3.80	0.950	4.10
TEM2	1.25	30	51.1	24.40	28.11	9.59	6630	9.555	4.90	1.300	3.25
TEM6	1.25	40	49.0	24.45	39.11	14.06	8790	8.611	3.30	0.850	3.95
TEM7	1.25	30	49.0	24.80	38.30	13.84	8610	8.525	4.35	1.100	3.25
EXP1	1.25	30	51.5	23.80	24.49	8.19	5740	9.881	4.72	1.195	3.37
EXP2	1.25	40	55.5	24.60	46.86	14.44	11714	11.545	4.46	1.063	4.61
EXP3	1.25	35	57.0	23.78	47.26	14.00	12100	12.465	5.72	1.123	4.20
EXP4	1.25	25	42.5	23.20	51.74	21.88	10370	6.205	5.00	0.945	3.06
EXP5	1.25	20	36.7	23.45	53.78	28.50	9660	3.972	4.41	0.708	2.63
EXP6	0.75	20	30.5	23.80	135.81	82.00	12910	1.840	1.40	0.218	2.58
EXP7	0.75	30	36.7	23.45	145.43	59.73	15680	3.972	1.81	0.302	4.15
EXP8	2.00	40	52.8	23.60	17.82	7.28	6830	10.521	5.16	1.750	3.92
EXP9	2.00	40	49.8	23.90	9.55	4.28	3480	9.097	3.20	1.055	4.47
EXP11	0.75	20	40.3	23.40	145.43	51.58	16715	5.307	3.48	0.542	2.42
EXP12	0.75	15	41.0	23.80	130.15	45.42	15233	5.478	4.82	0.625	1.83
EXP13	0.75	25	40.2	24.05	116.57	42.32	13396	5.113	2.63	0.441	3.02
EXP14	2.00	25	49.0	23.45	6.45	2.88	2318	8.852	4.62	1.664	2.95
EXP15	2.00	35	49.0	23.75	6.45	2.89	2318	8.781	2.91	1.060	3.92
EXP17	1.25	35	49.0	23.25	39.93	14.06	8980	8.899	4.35	0.995	4.08
EXP18	1.25	25	49.0	23.80	39.93	14.17	8980	8.769	6.19	1.288	3.02
FEB2	2.00	80	54.0	17.10	13.53	5.13	5305	12.369	1.90	0.670	8.45
FEB3	2.00	60	51.0	17.51	6.68	2.70	2520	10.930	1.70	0.661	6.75
FEB4	2.00	60	55.3	16.63	11.14	4.05	4450	13.053	2.75	0.950	6.75
FEB5	2.00	70	56.2	17.25	14.01	5.09	5600	13.387	2.60	0.900	6.60
FEB6	2.00	70	50.2	15.25	8.44	3.40	3125	10.908	1.53	0.680	7.45
FEB7	2.00	60	49.4	15.63	8.44	3.47	2910	10.503	2.05	0.817	7.06
APR1	2.00	55	49.0	16.85	6.61	2.76	2375	10.149	1.65	0.717	6.50
APR2	2.00	65	47.0	17.18	5.57	2.44	1955	9.237	1.23	0.520	6.33
APR3	2.00	75	47.0	17.38	5.33	2.34	1870	9.205	0.93	0.398	7.67
APR4	2.00	25	54.5	16.54	5.97	2.23	2360	12.690	6.30	2.210	2.89
APR5	2.00	35	54.5	16.82	5.57	2.09	2210	12.647	3.25	1.420	5.00
APR6	2.00	45	53.5	17.03	4.27	1.62	1670	12.147	1.46	0.760	7.00

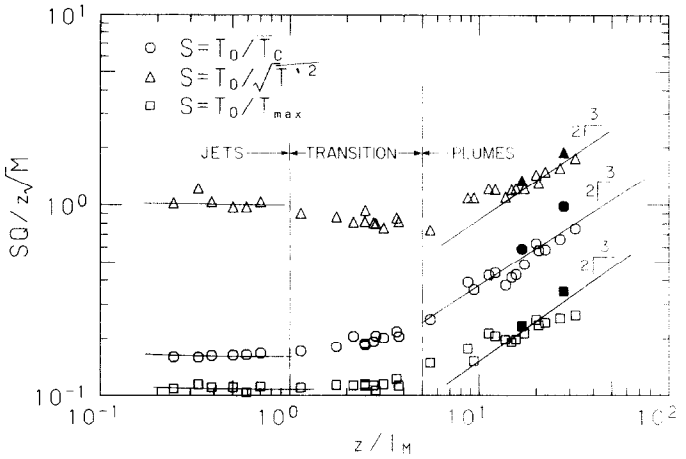

FIG. 4. Dimensionless mean (○), r.m.s. (△) and maximum (□) temperatures along the axis of a buoyant jet, vs the dimensionless elevation.

and

$$\frac{(T_0/\sqrt{(\overline{T'^2})})Q}{z\sqrt{M}} \sim \left(\frac{z}{l_M}\right)^{2/3}, \quad \text{for} \quad z/l_M > 5. \tag{6}$$

The transition in turbulence intensity fluctuations from a jet-like to a plume-like nature occurs in a very brief interval on the z/l_M axis. These decay laws for mean and turbulence temperatures on the axis of the jet are also followed by the instantaneous maximum temperature observed at the axis of the jet. The minimum excess temperatures observed at the jet axis were found to approach zero.

The normalized width $b_T(z)/z$ of the mean temperature profile as defined by the 1/e point is plotted vs the dimensionless elevation z/l_M in Fig. 5. The logarithmic abscissa is used in order to expand the jet regime for $z/l_M < 1$. For both small and large z/l_M (jet and plume flows) width is a linear function of the dimensionless distance from the source. However, there is a difference between the jet and plume growth as evident in the position of the straight line fitted to the data. The ratio b_T/z takes the constant values of 0.13 and 0.11 in jets and plumes, respectively, denoting a linear growth for the two asymptotic cases. The transition in the slope from 0.13 to 0.11 occurs in the interval $1 < z/l_M < 5$. It appears therefore that the linear growth of a buoyant jet as proposed by Kotsovinos [28] is not supported by these data. This can be attributed to the fact that the data he used were limited to about $z/l_M = 10$, so that the asymptotic plume regime was not reached adequately as is confirmed by his mean temperature and turbulence intensity on the axis, which follow the asymptotic plume properties beyond elevations $z/l_M = 6$ and 14, respectively.

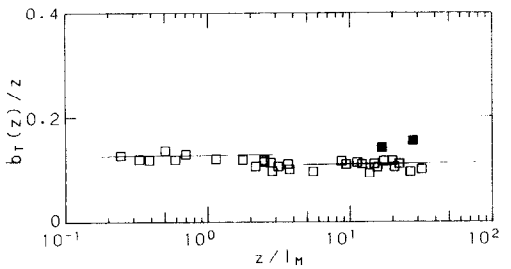

FIG. 5. Dimensionless 1/e temperature width indicating the angle of expansion of a buoyant jet.

The solid symbols in Figs. 4 and 5 correspond to plumes with initial plume Richardson numbers varying from about 0.7 to 1.0. Papanicolaou [20] reported a limiting plume Richardson number of 0.63. Hence for initial $R_0 > 0.63$ an adjustment zone must exist in which the plume reaches an asymptotic Richardson number. In this case a jet virtual origin located at some distance z_0 from the nozzle becomes important and the dimensionless elevation must be replaced by $(z+z_0)/l_M$.

3.2. *Statistical properties of the temperature across jets and plumes*

The time averaged excess temperature at a point (r, z) normalized by the mean centerline temperature is plotted vs r/z in Figs. 6(a) and (b) for jets and plumes, respectively. Measurements were performed up to 40 initial jet and plume diameters downstream from the jet source. The data are best fitted by the exponentials

$$\begin{aligned} \bar{T}/\bar{T}_c &= \exp[-75(r/z)^2] \quad \text{(jets)} \\ \bar{T}/\bar{T}_c &= \exp[-80(r/z)^2] \quad \text{(plumes)}. \end{aligned} \tag{7}$$

The normalized mean temperature profile for a jet agrees with that reported by Antonia *et al.* [13], Becker *et al.* [15], Birch *et al.* [16] and Shaughnessy and Morton [17]. For a plume the mean non-dimensional temperatures agree with the data of Zimin and Frik [25].

Although the normalized time-averaged mean temperature profiles are very similar in jets and plumes

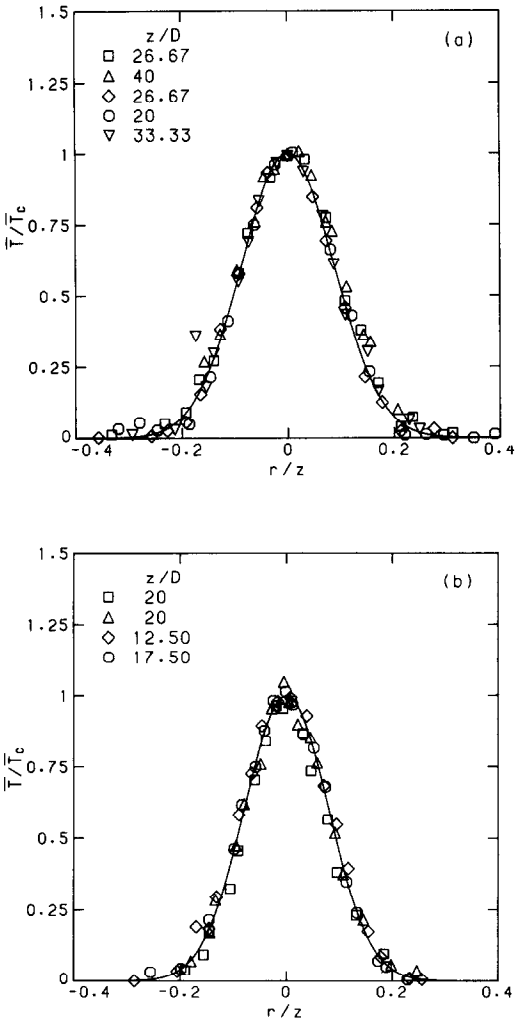

FIG. 6. Non-dimensional mean excess temperature profile (a) across a jet and (b) across a plume.

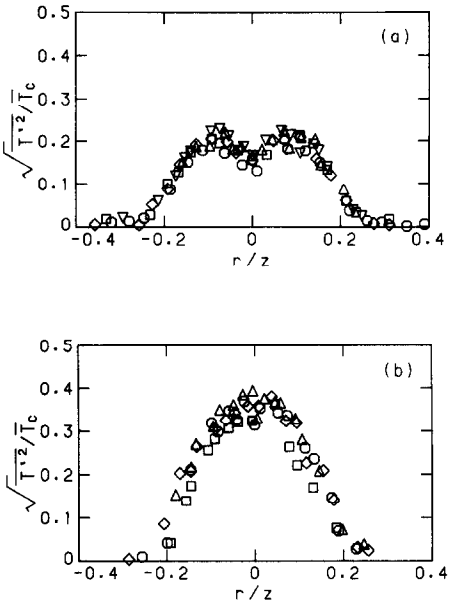

FIG. 7. Profile of the intensity of turbulent fluctuations of the temperature (a) across a turbulent jet, (b) across a plume (symbols as in Fig. 6).

the r.m.s. temperature fluctuation profiles are very different in each case. In Figs. 7(a) and (b) the r.m.s. temperature normalized by the mean temperature on the flow axis is plotted vs the dimensionless distance (r/z) from the axis for a jet and a plume, respectively. The normalized r.m.s. temperature in plumes is almost twice that measured in jets. The peak value in a plume (0.40) occurs on the axis, while in a jet it occurs at a distance $r/z = 0.070$ with a value of 0.25 and a centerline value of 0.15–0.18. Figures 7(a) and (b) show that the buoyancy amplifies the intensity of the turbulence of a passive scalar transported by the flow. The two peaks apparent in the intensity of turbulence observed in momentum driven jets tend to coalesce in plumes. The present results are similar to those reported by Becker *et al.* [15] and Birch *et al.* [16] for a jet regarding the magnitude and the location of the peak r.m.s. temperatures. Antonia *et al.* [13] (jet in a coflowing stream) reported values 0.25 and 0.35 at the axis and peak, respectively, appearing to indicate that ambient turbulence also amplifies the turbulent intensity. Chevray and Tutu [11] reported a slightly higher centerline turbulent intensity (0.20). Nakagome and Hirata [21] found a centerline value of 0.30 for their plume rising from a heated disc and George *et al.* [22] reported 0.35 around their plume axis. The present data also agree with Kotsovinos' [28] results concerning the r.m.s. values observed in jets and plumes.

The normalized maximum and minimum temperatures at different radial locations are plotted vs r/z in Figs. 8(a) and (b) for a jet and a plume, respectively. The minimum temperature observed anywhere in a plume was zero, but this was not the case in jets. Maximum temperatures occur on the flow axis and were found to vary from 1.50 times the mean centerline temperature in jets to 2.50 times the mean in plumes. The present results are in agreement with those reported by Kotsovinos [29] for the case of the plane jets and plumes.

3.3. *Probability density functions, spectra of turbulence*

For a discrete temperature turbulent signal, the probability $P(T, T+\delta T)$ of the temperature in the interval $(T,\ T+\delta T)$ is the ratio of the number of temperature data points which occurred in this interval divided by the total number of data points recorded. The probability density distribution (pdf) then is the ratio $P(T, T+\delta T)/\delta T$ for this interval. Accurate pdfs can be derived from long records where sampling is performed at high rates. Normalizing the temperature interval by the mean axial temperature to give $(T-T_a)/\bar{T}_c$ results in a variable that takes values between zero and the normalized local

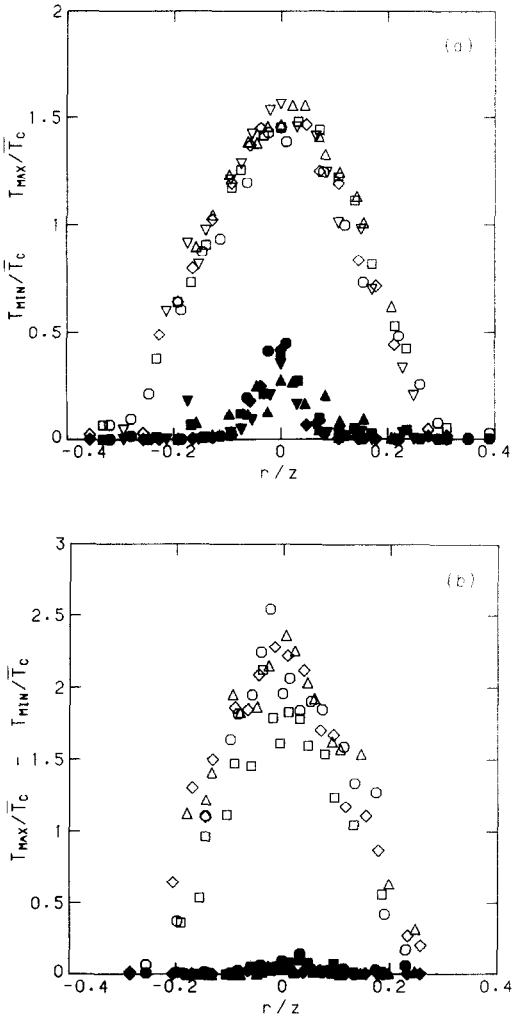

FIG. 8. Profile of the maximum (open symbols) and the minimum (solid symbols) excess temperatures observed across (a) jets and (b) plumes (symbols as in Fig. 6).

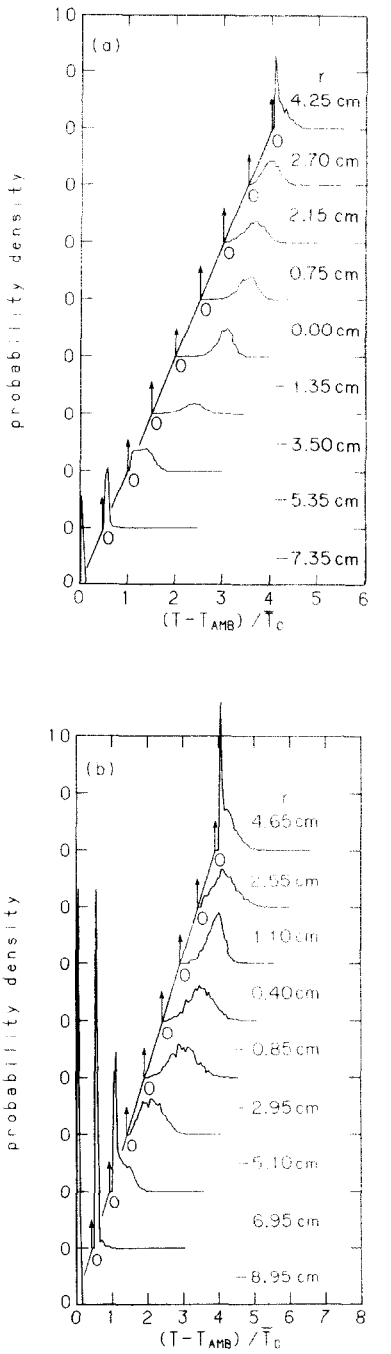

FIG. 9. Probability density distribution of the excess temperature (a) across a jet $z/D = 33.33$, (b) across a plume $z/D = 17.50$.

maximum temperature, as shown in Figs. 9(a) and (b).

These figures show the change of the pdf as a function of the normalized radial distance r/z in a jet and a plume, respectively, at 26.67 and 17.50 diameters downstream from the jet exit. In a jet, the pdf is roughly Gaussian with increasing variance for $r/z < 0.10$. Beyond this radial distance the flow is highly intermittent and the pdf becomes asymmetrical approaching a δ-function at the jet boundary. Plumes have similar behavior as shown in Fig. 9(b). The normalized probability density function for temperature fluctuations on the flow axis is plotted in Figs. 10(a) and (b) for jets and plumes, respectively. The plotted data correspond to different experiments with different initial conditions and display self-similarity in the probability density function on the flow axis. The probability density takes higher values in jets than in plumes, because the variance of the temperature fluctuations is smaller in jets as is to be expected from Figs. 8(a) and (b).

In Figs. 11 (a) and (b) the power spectral density of the temperature is plotted vs the frequency of the temperature signal. The power spectra were calculated using the Fast Fourier Transform algorithm with 10 000 data points sampled at a rate of 80 samples per second (the maximum allowed rate by the thermistor response time of 0.014 s and the thermistor tip size

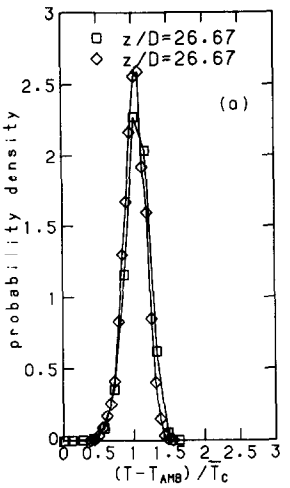

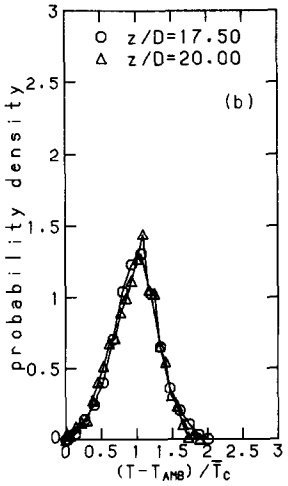

FIG. 10. Probability density distribution of the temperature on the axis (a) jet, (b) plume.

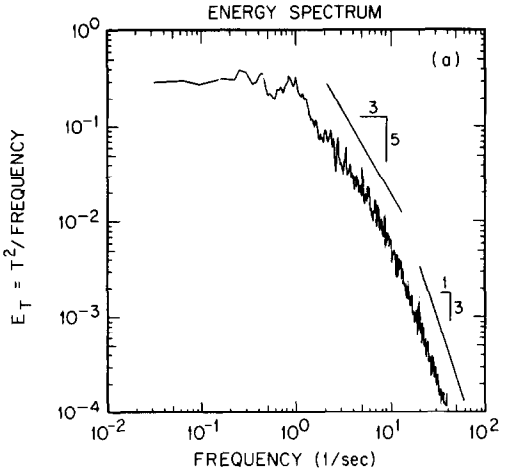

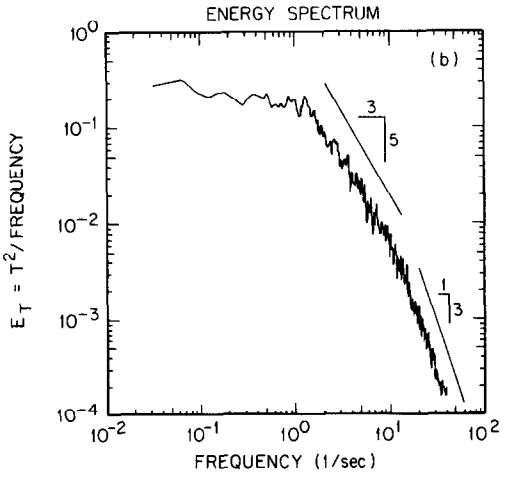

FIG. 11. Power spectral density distribution of the r.m.s. temperature in a buoyant jet $z/D = 53$, $z/l_M = 1.52$, (a) at the centerline, (b) at $r/z = 0.05$.

0.20 mm). The measurements were performed at the centerline and at $r/z = 0.05$ and at a location 53 jet diameters downstream from the nozzle of a heated jet in the transition region with $z/l_M = 1.52$. From both cases a $-5/3$ decay of the spectral energy is observed for frequencies of 1–10 Hz. Since the fluid is water, and the local Prandtl number takes a value of 7 the slope of the spectrum at higher frequencies (towards the viscous convective subrange) should approach -1. This is a result based on dimensional arguments (see Tennekes and Lumley [32] and Townsend [33]) for a passive scalar transported by the flow. In the above figures the slope of the spectrum becomes -3 rather than -1. This same spectral density decay was observed by Papanicolaou [20] for salinity produced buoyancy, where the scalar was a fluorescent dye transported by the flow. It has also been reported by Mizushina *et al.* [34] and Ramaprian and Chandrasekhara [35] for buoyant flows where the scalar was temperature and the local flow Richardson number was high. It appears that for buoyancy driven flows where the local Richardson number is high, the viscous convective subrange ($Pr \gg 1$) is substituted by an inertial diffusive subrange in the equilibrium spectra as if the local Prandtl number was $Pr \ll 1$. This will be discussed further subsequently.

The intermittency factor γ is plotted vs r/z in Figs. 12(a) and (b) for a jet and a plume, respectively. The intermittency factor was calculated as the ratio of the time that mixed fluid was apparent at a point in the flow field over the overall sampling time. The threshold temperature above which the fluid was assumed to be mixed was taken to be 0.05°C above the ambient temperature. The intermittency factor is one for $r/z < 0.15$ in jets and for $r/z < 0.10$ in plumes, implying that the ambient fluid is entrained and remains unmixed closer to the axis in plumes than in jets. This was shown by the dimensionless temperature maxima and minima profiles in jets and plumes presented earlier.

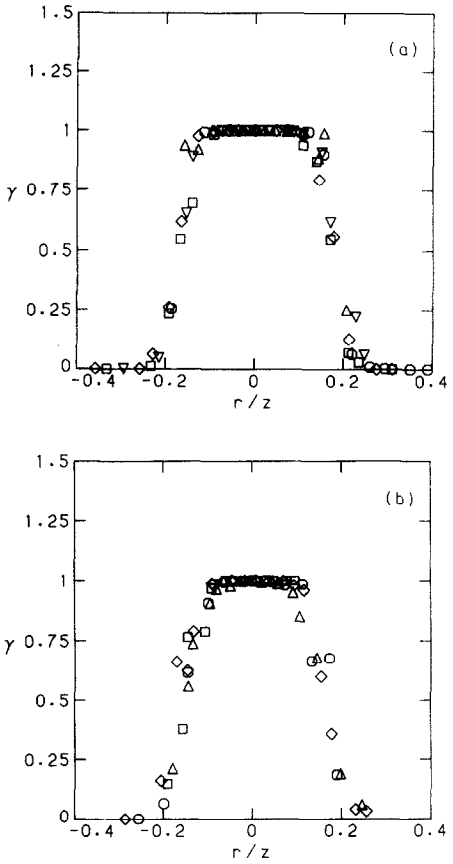

FIG. 12. Intermittency factor of the temperature distribution (a) across a jet, (b) across a plume (symbols as in Fig. 6).

Since the flow is intermittent it is possible to split the turbulence intensity into two separate parts, one due to the existence of mixed fluid at the point of interest and the other due to the existence of ambient fluid there. Figures 13(a) and (b) and 14(a) and (b)

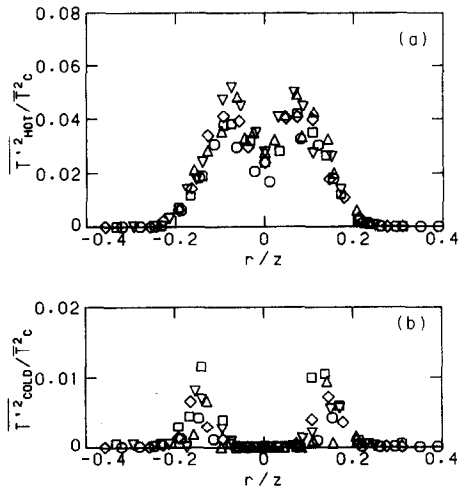

FIG. 13. Intensity of turbulence across a turbulent jet of (a) the mixed (hot) fluid, (b) the unmixed (cold) ambient fluid (symbols as in Fig. 6(a)).

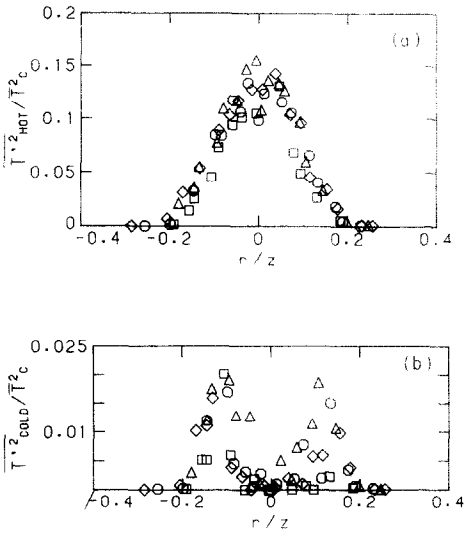

FIG. 14. Intensity of turbulence across a plume of (a) the mixed (hot) fluid, (b) the unmixed (cold) ambient fluid (symbols as in Fig. 6(b)).

are the dimensionless plots of the normalized mixed fluid and ambient fluid turbulent temperature in jets and plumes, respectively. The ambient (cold) fluid turbulence intensity takes its maximum value at the radial distance from the jet axis where the intermittency factor drops below one. Also these peak values occur at the same radial distance as the

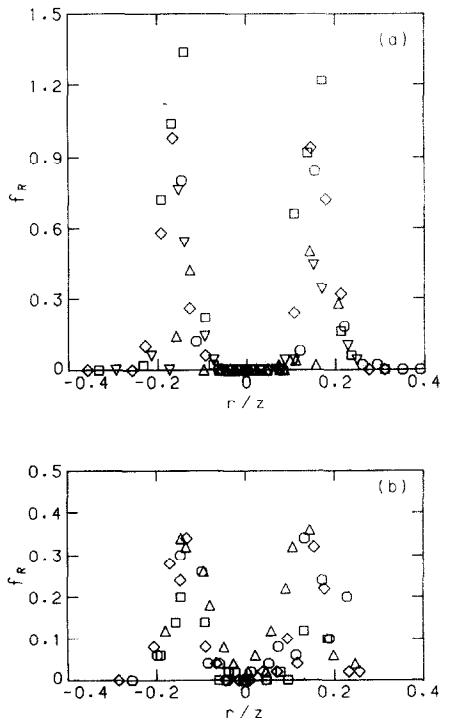

FIG. 15. Frequency of crossing of the hot–cold interface in (a) jets, (b) plumes (symbols as in Fig. 6).

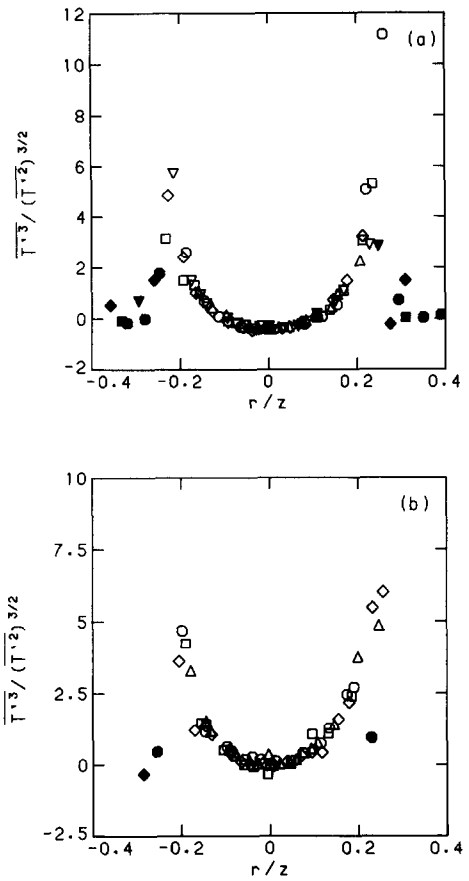

FIG. 16. Skewness factor across (a) turbulent jets, (b) plumes (symbols as in Fig. 6). Solid symbols correspond to data points with low signal-to-noise ratio.

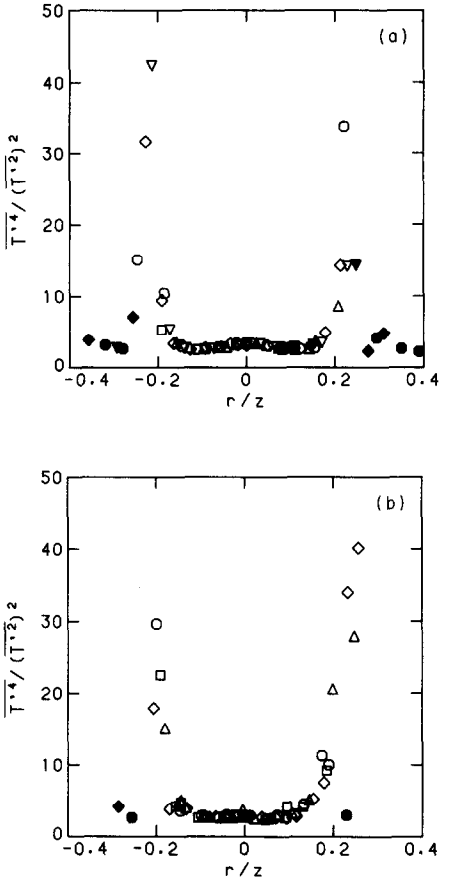

FIG. 17. Flatness factor across (a) turbulent jets, (b) plumes (symbols as in Fig. 6). Solid symbols correspond to data points with low signal-to-noise ratio.

observed maxima of the frequency of the hot–cold interface crossing as shown in Figs. 15(a) and (b) for jets and plumes, respectively. It is clear that f_R for jets is twice that for plumes. This is in agreement with Kotsovinos' [36] observations for plane buoyant jets. It is also indicative of the existence of slower moving large eddies in plumes compared to the faster large coherent structures in jets.

The third and fourth moments of the turbulent signal are plotted in Figs. 16(a) and (b) and 17(a) and (b) for jets and plumes, respectively, vs the dimensionless distance r/z from the axis. The normalized third moment (skewness factor) on the axis takes a value close to zero and the normalized fourth moment (flatness factor) a value of three verifying the Gaussian distribution of the temperature fluctuations at this location.

4. DISCUSSION AND CONCLUSIONS

The experimental results presented in the foregoing appear to provide a reasonably sound basis for the dimensional arguments commonly used to define jet and plume behavior in the mean. It is clear that jets with buoyancy do develop asymptotically into plumes as predicted by these dimensional arguments. The length scale l_M is a well-defined measure of the distance at which this transition occurs. The somewhat surprising result is that the turbulence intensities scale in a similar fashion to the time-averaged mean tracer concentrations on the axis of both jets and plumes. Given that there are two mechanisms for turbulent kinetic energy production in plumes and only one in jets this is interesting. With turbulent jets the shear production of turbulent kinetic energy results in a net loss in mean flow kinetic energy as the jet progresses from the source, even though to a first approximation, momentum is conserved. In a plume, buoyant forces feed energy directly into the mean kinetic energy to replace that lost by shear production. They also provide a direct source of energy into the turbulent kinetic energy balance. Thus it is not surprising to find the relative intensity of turbulence fluctuations to be higher in plumes than occurs in jets. This is also evident in the profiles of relative maximum instantaneous tracer concentration. These results are similar to those reported by Kotsovinos [28, 36] for two-dimensional and round buoyant jets. The growth in the width of

the mean tracer profile does appear to be different in jets and plumes, notwithstanding the conclusion by Kotsovinos and List [19] for plane jets and plumes that the growth rates are the same. An explanation for this must be evident in the analysis of entrainment mechanisms appropriate for jets and plumes, which will be the subject of a subsequent paper.

Where the real difference between jets and plumes becomes apparent is in the spectral estimates of energy distribution in the fluctuations. The existence of buoyancy driven motions in the turbulent flow appears to suppress the conductive range in a flow where the Schmidt number is larger than unity. The spectral density decays faster than the $-5/3$ power of the wave number and contradicts the theoretical predictions at higher wave numbers. The decay of the spectral flux of the temperature fluctuations is in accordance with theoretical arguments for the inertial diffusive subrange. It can be argued that the cause of the local dissipation of the temperature variance in buoyancy driven flows is the buoyancy generated inertia forces rather than the viscous forces.

The evolution from buoyant jets to plumes is associated with higher mean dilutions resulting in larger volumes of ambient unmixed fluid being entrained and finally mixing with the plume fluid. This is in accordance with larger coherent structures apparent in plumes, which entrain unmixed ambient fluid that can reach the flow axis. This becomes evident from the minimum temperatures observed locally in plumes being zero everywhere. Also, the intermittency factor profile evolves becoming narrower for large values of z/l_M and the frequency of hot–cold interface crossing is nonzero around the plume axis. A physical consequence of the large coherent structures existing in a plume is a reduction in mobility due to the rapid inertial growth of the moving masses of fluid. Although the turbulence is non-isotropic in a buoyant jet the probability distribution of the temperature could be approximated by a Gaussian. The buoyancy produced momentum broadens the variance and reduces the maximum value of the 'Gaussian probability density' as it becomes dominant for $z/l_M > 1$.

The present results support the dimensional arguments associated with the transition from jets to plumes satisfactorily. However, the evolution of the plume flow may not be complete since the present experiment was limited to 40 initial plume diameters from the source. Questions such as, does the intermittency factor profile evolve further in a plume taking values well below unity around the axis, or, does the plume growth become nonlinear, or, is the jet-like flow under consideration self-similar, are still not fully resolved. These questions are related to the inability of intrusive probe-based measuring techniques to resolve the temperature, salinity or other tracer concentration very far from the jet source. Regardless of these limitations the present investigation does provide adequate experimental constants to describe the dispersion of plumes for engineering applications. Experiments were limited to 40 jet and plume diameters because the initial excess temperature produced buoyancy at the source which rapidly converted a jet to a plume, thus limiting the measurement in the jet regime. At the same time accelerated plume dilution limited measurements in the buoyancy dominated flow regime. In this case a rapid buoyancy drop at the initial stages of flow due to the nonlinearity of the thermal expansion coefficient of water, is equivalent to a change of the jet initial conditions. It is evidently necessary to develop a better technique which will result in accurate dilution measurements in both jets and plumes within the self-similar regime of the flow far from the source.

Acknowledgment—The authors gratefully acknowledge the financial support of the National Science Foundation through Grant No. CEE-8117272.

REFERENCES

1. B. R. Morton, G. I. Taylor and J. S. Turner, Turbulent gravitational convection from maintained and instantaneous sources, *Proc. R. Soc. London* **A234,** 1–23 (1956).
2. G. K. Batchelor, Heat convection and buoyancy effects on fluids, *Q. J. R. Met. Soc.* **80,** 339–358 (1954).
3. H. B. Fischer, E. J. List, R. C. Y. Koh, J. Imberger and N. H. Brooks, *Mixing in Inland and Coastal Waters.* Academic Press, New York (1979).
4. S. Corrsin, Investigation of flow in an axially symmetric heated jet of air, NACA Wartime Rept. W-94 (1943).
5. S. Corrsin and M. S. Uberoi, Further experiments on the flow and heat transfer in a heated turbulent air jet, NACA Rept. 998 (1950).
6. J. O. Hinze and B. G. van der Hegge Zijnen, Transfer of heat and matter in the turbulent mixing zone of an axially symmetric jet, *Appl. Scient. Res.* **A1,** 435–461 (1949).
7. W. Forstall and E. W. Gaylord, Momentum and mass transfer in a submerged water jet, *J. Appl. Mech.* **22,** 161–164 (1955).
8. P. D. Sunavala, C. Hulse and M. W. Turing, Mixing and combustion in free and enclosed turbulent jet diffusion flumes, *Combust. Flame* **1,** 79–193 (1957).
9. K. M. Kiser, Material and momentum transport in axisymmetric turbulent jets of water, *A.I.Ch.E. Jl* **9,** 386–390 (1963).
10. R. A. M. Wilson and P. V. Danckwerts, Studies in turbulent mixing II: a hot air jet, *Chem. Engng Sci.* **19,** 885–895 (1964).
11. R. Chevray and N. K. Tutu, Intermittency and preferential transport of heat in a round jet, *J. Fluid Mech.* **88,** 133–160 (1978).
12. P. M. Sforza and R. F. Mons, Mass, momentum and energy transport in turbulent free jets, *Int. J. Heat Mass Transfer* **21,** 371–384 (1978).
13. R. A. Antonia, A. Prabhu and S. E. Stephenson, Conditionally sampled measurements in a heated turbulent jet, *J. Fluid Mech.* **72,** 455–480 (1975).
14. H. A. Becker, H. C. Hottel and G. C. Williams, On the light-scattering technique for the study of turbulence and mixing, *J. Fluid Mech.* **30,** 259–284 (1967).
15. H. A. Becker, H. C. Hottel and G. C. Williams, The nozzle-fluid concentration field of the round turbulent free jet, *J. Fluid Mech.* **30,** 285–303 (1967).
16. A. D. Birch, D. R. Brown, M. G. Dodson and J. R. Thomas, The turbulent concentration field of a methane jet, *J. Fluid Mech.* **88,** 431–449 (1978).
17. E. J. Shaughnessy and J. B. Morton, Laser light-scattering measurements of particle concentration in a turbulent jet, *J. Fluid Mech.* **80,** 129–148 (1977).

18. H. Rouse, C. S. Yih and H. W. Humphreys, Gravitational convection from a boundary source, *Tellus* **4**, 201–210 (1952).
19. N. E. Kotsovinos and E. J. List, Plane turbulent buoyant jets: Part 1—integral properties, *J. Fluid Mech.* **81**, 25–44 (1977).
20. P. N. Papanicolaou, Mass and momentum transport in a turbulent buoyant vertical axisymmetric jet, Report No. KH-R-46, W. M. Keck Laboratory of Hydraulics and Water Resources, California Institute of Technology, Pasadena, California (1984).
21. H. Nakagome and M. Hirata, The structure of turbulent diffusion in an axisymmetric thermal plume. *Proc 1976 ICHMT Seminar on Turbulent Buoyant Convection*, pp. 361–372. Hemisphere, Washington, DC (1976).
22. W. K. George, R. L. Alpert and F. Tamanini, Turbulence measurements in an axi-symmetric buoyant plume, *Int. J. Heat Mass Transfer* **20**, 1145–1154 (1977).
23. I. Wygnanski and H. Fiedler, Some measurements in the self-preserving jet, *J. Fluid Mech.* **38**, 577–612 (1969).
24. G. Abraham, Jet diffusion in liquid of greater density, *Proc. ASCE, J. Hyd. Div.* **86**, 1–13 (1960).
25. V. D. Zimin and P. G. Frik, Averaged temperature fields in asymmetrical turbulent streams over localized heat sources, *Izv. Akad. Nauk. SSSR, Mekhanika Zhidkosti Gaza* **2**, 199–203 (1977).
26. F. Ogino, H. Takeuchi, I. Kudo and T. Mizushina, Heated jet discharged vertically into ambients of uniform and linear temperature profiles, *Int. J. Heat Mass Transfer* **23**, 1581–1588 (1980).
27. J. C. Chen and W. Rodi, *Vertical Turbulent Buoyant Jets: a Review of Experimental Data*. Pergamon Press, Oxford (1980).
28. N. E. Kotsovinos, Temperature measurements in a turbulent round plume, *Int. J. Heat Mass Transfer* **28**, 771–777 (1985).
29. N. E. Kotsovinos, A study of the entrainment and turbulence in a plane jet, Report No. KH-R-32, W. M. Keck Laboratory of Hydraulics and Water Resources, California Institute of Technology, Pasadena, California (1975).
30. R. G. Lueck, O. Hertzman and T. I. Osborn, The spectral response of thermistors, *Deep-Sea Res.* **24**, 951–970 (1977).
31. M. C. Gregg and T. B. Meagher, The dynamic response of glass rod thermistors, *J. Geophys. Res.* **85**(C5), 2779–2786 (1980).
32. H. Tennekes and J. L. Lumley, *A First Course in Turbulence*. MIT Press, Cambridge, Massachusetts (1972).
33. A. A. Townsend, *The Structure of Turbulent Shear Flows*, 2nd Edn. Cambridge University Press, London (1976).
34. T. Mizushina, F. Ogino, H. Veda and S. Komori, Application of laser-Doppler velocimetry to turbulence measurement in non-isothermal flow, *Proc. R. Soc. London* **A366**, 63–79 (1979).
35. B. R. Ramaprian and M. S. Chandrasekhara, Study of vertical plane turbulent jets and plumes, IIHR Report No. 257, Iowa Institute of Hydraulic Research (1983).
36. N. E. Kotsovinos, Plane turbulent buoyant jets: Part 2—turbulence structure, *J. Fluid Mech.* **81**, 45–62 (1977).

PROPRIETES STATISTIQUES ET SPECTRALES DE CONCENTRATION EN TRACEUR DANS DES JETS CIRCULAIRES FLOTTANTS

Résumé—La croissance spatiale, la décroissance de la température, et la structure de turbulence ont été étudiées expérimentalement dans des jets flottants axisymétriques en transition vers les panaches et dans les écoulements-panaches pleinement établis. Des enregistrements de température obtenus avec des thermistors à réponse rapide placés dans ces écoulements constituent la base de cette analyse. Les résultats obtenus soutiennent des arguments asymptotiques antérieurs à la vitesse de décroissance de la température moyenne et des fluctuations de moyenne quadratique de la température. Des distributions spectrales d'énergie dans des jets et des panaches montrent que l'évolution depuis les jets flottants vers les panaches est caractérisée par un glissement sensible dans la distribution du nombre d'onde de la densité de variance de la température.

STATISTISCHE UND SPEKTRALE EIGENSCHAFTEN DER TRACERKONZENTRATION IN AUFTRIEBSFREISTRAHLEN MIT KREISQUERSCHNITT

Zusammenfassung—Ausbreitung, Temperaturabfall und Struktur der Turbulenz in axialsymmetrischen Auftriebsfreistrahlen beim Übergang zur reinen Auftriebsströmung und in der voll entwickelten Auftriebsströmung wurden experimentell untersucht. Temperaturmessungen mit in der Strömung eingebauten Thermistoren geringer Ansprechzeit bilden die Grundlage für die Studie. Die Ergebnisse stützen frühere Näherungsthesen über den Temperaturabfall und die Temperaturschwankungen. Spektrale Energieverteilungen in Freistrahlen und Auftriebsströmungen zeigen, daß der Übergang vom einen ins andere durch eine erhebliche Änderung der Wellenzahlverteilung der Temperaturvarianzdichte gekennzeichnet ist.

СТАТИСТИЧЕСКИЕ И СПЕКТРАЛЬНЫЕ ХАРАКТЕРИСТИКИ КОНЦЕНТРАЦИОННОГО СЛЕДА С СВОБОДНОКОНВЕКТИВНЫХ КРУГЛЫХ СТРУЯХ

Аннотация—Проведено экспериментальное исследование пространственного расплывания температуры и турбулентной структуры осесимметричных свободноконвективных течений при переходе к струйным течениям. Исследования основаны на термограммах, полученных с помощью высокочувствительных термисторов, обтекаемых этими потоками. Полученные результаты подтверждают асимптотические данные, относящиеся к расплыванию осредненной температуры и среднеквадратичных значений температурных флуктуаций. Спектральные распределения энергии в свободноконвективных и струйных течениях показывают, что эволюция свободноконвективных течений в струйные характеризуется значительным сдвигом в распределении по волновым числам интенсивности температурных флуктуаций.